Version 5 NOV 09

Electron-doping versus antisite defects: Structural and magnetic properties of $Sr_{2-x}La_xCrMoO_6$ and $Sr_{2-x}La_xCr_{1+x/2}Mo_{1-x/2}O_6$ perovskites.

J. Blasco[1], C. Ritter[2], J. A. Rodríguez-Velamazán[1,2] and J. Herrero-Martín[3].

[1]Instituto de Ciencia de Materiales de Aragón, CSIC-Universidad de Zaragoza, Departamento de Física de la Materia Condensada, Pedro Cerbuna 12, 50009 Zaragoza, Spain

[2]Institut Laue-Langevin, Grenoble Cedex 38042, France.

[3]European Synchrotron Radiation Facility, Boîte Postale 220, Grenoble Cedex 38042, France.

PACS: 71.30.+h, 75.30.kz, 75.47.Gk, 72.25.Ba

Keyworsds: Spintronic, magnetoresistance, electron doping, antiferrimagnetism, double perovskite

Corresponding author: Javier Blasco Carral.

I C M A- Departamento de Física de la Materia Condensada

CSIC - Universidad de Zaragoza.

C/ Pedro Cerbuna 12, 50009 Zaragoza. Spain.

e-mail: jbc@unizar.es

Abstract

This study reports the synthesis, structure and magnetic properties of a set of $Sr_{2-x}La_xCrMoO_6$ and $Sr_{2-x}La_xCr_{1+x/2}Mo_{1-x/2}O_6$ samples. Although both series exhibit similar crystal structures, $Sr_{2-x}La_xCrMoO_6$ samples present an effective electron doping revealed by a significant expansion of the unit cell with increasing x. In $Sr_{2-x}La_xCr_{1+x/2}Mo_{1-x/2}O_6$ samples instead, the Cr-excess leads to a non electron doped system. Both series show a large amount of antisite defects whose number increases as La-content increases. Neutron diffraction patterns reveal the existence of long range magnetic ordering for all samples but the magnetic peaks are very broad for Sr_2CrMoO_6 indicating a short coherence length for the magnetic phase. This coherence length is increased upon replacing Sr by La. In both systems (electron doped and non electron doped) there is a clear increase of the magnetic transition temperature with doping. The samples show ferromagnetic contributions at low temperature as deduced from the magnetic hysteresis loops typical of hard ferromagnetic materials. However, magnetic saturation is not achieved even at 5 T and the magnetic moment at this field is very small. The ac magnetic susceptibility reveals the existence of several anomalies suggesting that these compounds are magnetically inhomogeneous. This is probably due to the presence of the large amount of antisite defects not homogenously distributed.

1. Introduction.

The study of half metals having only one spin direction at the Fermi level is of great interest in the field of spintronics [1]. Among these compounds, magnetic double perovskites (DP) are very promising owing to their high Curie temperature (T_C) and the predicted half-metallic character for the ground state [2]. These compounds are nominally $A_2BB'O_6$ and we denote them as BB'-based DP. A stands for a big cation (usually alkaline earth or rare earth) whereas B and B' are two different transition metals which are arranged as rock-salt in the primitive perovskite B-site giving rise to two new sublattices. The ordering is favoured by large differences in either atomic size or valence state between B and B' [3,4].

The most studied DP is by far Sr_2FeMoO_6 [2,5-10]. In this compound electron doping (e-doping), achieved by partial substitution of Sr^{2+} with La^{3+} (or another light rare earth), gives rise to an enhancement of T_C [7-10]. The result was confirmed in other FeMo-based compounds [11] and opened expectations of obtaining robust half-metals suitable for high temperature devices. Unfortunately, this type of substitution also induces structural changes which make difficult to discern the purely electronic effects associated to doping from structural impacts. One undesirable structural effect is the increase of anti-site defects (ASD) in doped samples. These defects stand for misplaced B ions which occupy the ideal position of B' ones (and vice versa). ASD are quantified by the percentage of misplaced ions in such a way that ASD= 0% corresponds to a fully ordered DP whereas ASD is 50% for a single perovskite with the two cations randomly distributed.

ASD of 15% are usually reported for undoped Sr_2FeMoO_6 whereas it reaches values around 40% for $Sr_{1.5}La_{0.5}FeMoO_6$ [12]. Such a high amount of ASD implies a strong contribution of the direct Fe-O-Fe superexchange interactions to the magnetic

properties of the sample and therefore this type of interactions has been suggested by some authors as the principal driving force for the T_C-enhancement in e-doped DP [13]. The exact role of e-doping in determining the physical properties of DP had to be questioned as well on the basis of results obtained in other DP systems. Recent reports on CrW-based compounds have shown for example a strong T_C decrease with e-doping [14]. In MnW-based DP the e-doping seems to increase ferromagnetic correlations but the doped compounds do not develop long range magnetic ordering [15].

Trying to increase T_C through e-doping by substitution is furthermore confronted with the basic problem of incorporating the substituting ion successfully into the matrix. A recent detailed study showed e.g. that the attempted synthesis of the system $Sr_{2-x}La_xCrReO_6$ was unsuccessful [16] due to the formation of competitive $Sr_{2-x}La_xCr_{1+x/2}Re_{1-x/2}O_6$ phases [16, 17]. In this case, the additional electrons injected by La^{3+} are compensated by the increase of the Cr^{3+} ratio (compared to Re^{5+}), leading to a non e-doped system.

Recently we were successful in preparing e-doped samples in FeRe-based system [18]. The samples showed a low amount of ASD and a T_C-enhancement with e-doping. These results support the suitability of this kind of doping to increase T_C in some DP. For the moment it seems that this effect can be clearly observed in FeMo- and FeRe-based systems but the situation is not obvious at all for DP without Fe.

Further studies are therefore needed to learn more about the possibilities of this type of e-doping in DP and to discern the effects produced in different systems. In order to do so we are now focusing our attention on CrMo-based DP for several reasons. Firstly, there are not reports about the existence of $Sr_{2-x}La_xCrMoO_6$ samples and its study allows spreading out the research field of e-doped DP. Secondly, the

lighter transition metal in this system is Cr, not Fe, and the attempts of increasing T_C with doping in other Cr-based DP have failed due to reasons previously mentioned [14,17]. The study of CrMo-based compounds could shed light on the role of Cr atoms in the possibility of e-doping in DP.

The properties of Sr_2CrMoO_6 have been studied in the past reporting contradictory results. Moritomo et al. found ferrimagnetism in this DP with a low magnetic saturation at 5 K and T_C~300 K. The optical conductivity also suggested the presence of Cr^{3+} and Mo^{5+} valence states for this compound [19]. However, Arulraj et al. reported a ferrimagnetic transition at 450 K with a small ferromagnetic component [20] whereas Q. Lim et al. suggested that this DP shows an antiferromagnetic transition at T_N=40 K [21]. This variety of results may arise from the fact that Sr_2CrMoO_6 samples can be obtained with significant structural defects, mainly oxygen vacancies, and a large amount of ASD [22]. The presence of these imperfections strongly affects the properties of this DP [23]. In particular, the high level of ASD (around 35 %) leads to an increase in the number of direct of Cr-O-Cr (and Mo-O-Mo) interactions due to the structural disorder. In order to address this point, we have also studied the properties of the $Sr_{2-x}La_xCr_{1+x/2}Mo_{1-x/2}O_6$ series for the sake of comparison. In this series the substitution of Sr by La is accompanied by an effective increase of Cr-O-Cr interactions in such a way that the end-members of this series are the DP Sr_2CrMoO_6 on the one side and the single perovskite $LaCrO_3$ on the other. $LaCrO_3$ exhibits long antiferromagnetic ordering at T_N~300 K due to the Cr-O-Cr coupling [24].

The purpose of this work is to study the structural and magnetic properties of both series, with and without formal e-doping, in order to gain insight into the existence and effectiveness of this doping in Cr-based DP.

2. Experimental section.

$Sr_{2-x}La_xCrMoO_6$ ($x \leq 0.5$) and $Sr_{2-x}La_xCr_{1+x/2}Mo_{1-x/2}O_6$ ($x \leq 1$) compounds were synthesized by solid state reaction. Stoichiometric amounts of La_2O_3, $SrCO_3$, Cr_2O_3, MoO_3 and Mo were mixed, ground and heated at 1200º C for 2h in a current flow of Ar. We note that the physical behaviour of CrMo-based DP can be strongly influenced by the presence of oxygen vacancies [22]. In order to minimize the occurrence of this phenomenon we synthesized the compounds in an inert atmosphere with different Mo/MoO_3 ratios. Under these conditions we obtained the perovskite phase and secondary phases. The impurities were then successfully removed by sintering the compounds at high temperature with a small amount of H_2. The powder was pressed into pellets and sintered at 1400º C for 3 h in a stream of H_2/Ar (0.4:99.6). This step was repeated, if necessary, until the end of chemical reaction was indicated by the absence of changes in the x-ray patterns. We note that the amount of H_2 here used was five times lower than in our previous synthesis reported in ref. 22 which had a strong influence on the oxygen stoichiometry as we will see later.

The samples were characterized by x-ray powder diffraction (XRD) using a Rigaku D-Max system with Cu K_α radiation. Neutron powder diffraction data were measured at the Institut Laue Langevin (Grenoble, France) using two instruments. The high intensity diffractometer D1B with $\lambda \sim 2.52$ Å was used to perform temperature scans between 2 and 320 K. Meanwhile, the high resolution diffractometer D1A with $\lambda \sim 1.91$ Å was used to carry out crystal refinements at selected temperatures. Structures were refined by the Rietveld method using the Fullprof package program [25].

The chemical composition of the samples was tested by using the wavelength

dispersive x-ray fluorescence spectrometry technique (advant'XP+ model manufactured by Applied Research Laboratories). Magnetic measurements were carried out using a commercial Quantum Design superconducting quantum interference device (SQUID) magnetometer. The isothermal magnetization was determined at selected temperatures between -50 and 50 KOe. DC magnetization at 5 KOe was measured between 5 and 350 K and ac magnetic susceptibility was measured in the same range using an alternating field of 4 Oe and a frequency of 10 Hz.

3. Results and discussion.

3.1. Structural characterization

$Sr_{2-x}La_xCrMoO_6$ ($x \leq 0.5$) and $Sr_{2-x}La_xCr_{1+x/2}Mo_{1-x/2}O_6$ ($x \leq 1$) were obtained as black powders whose x-ray patterns are typical of a perovskite structure as shown in Figure 1 for $Sr_{2-x}La_xCrMoO_6$ samples. $Sr_{2-x}La_xCrMoO_6$ samples with $x \geq 0.6$ showed secondary phases, mainly $La_{1-x}Sr_xCrO_4$ and Mo, as also indicated in Fig 1. Superstructure peaks arising from the Cr/Mo rock-salt ordering are hardly noticeable for Sr_2CrMoO_6 and $Sr_{1.9}La_{0.1}CrMoO_6$ samples whereas they are not detected for $x \geq 0.2$ and the whole $Sr_{2-x}La_xCr_{1+x/2}Mo_{1-x/2}O_6$ series. In these cases, x-ray patterns are typical of a single perovskite.

In this type of compounds, oxygen atoms play an important role in the magnetic interactions so that it is desirable an accurate determination of both oxygen stoichiometry and atomic coordinates. It is well known that neutron diffraction is more sensitive to oxygen atoms than conventional x-ray diffraction so that we have made use of neutron diffraction to perform the crystal characterization on selected samples. The study was focused on Sr_2CrMoO_6, the e-doped compounds

$Sr_{1.9}La_{0.1}CrMoO_6$, $Sr_{1.7}La_{0.3}CrMoO_6$ and $Sr_{1.5}La_{0.5}CrMoO_6$ and finally, the non-doped samples $Sr_{1.7}La_{0.3}Cr_{1.15}Mo_{0.85}O_6$ $Sr_{1.5}La_{0.5}Cr_{1.25}Mo_{0.75}O_6$ and $SrLaCr_{1.5}Mo_{0.5}O_6$. In order to limit the number of free parameters, the samples were measured at high temperature in the paramagnetic region in order to refine the oxygen stoichiometry and the amount of ASD. These parameters were then fixed in the refinements performed at low temperature. The unit cells and refinement details are illustrated in the tables 1 and 2 for the measurements at 300 and 2 K, respectively. The atomic coordinates, occupancies at the B-sites, selected bond lengths and bond-angles are summarized in tables 3 and 4.

3.1.1. Sr_2CrMoO_6

Neutron patterns for this compound were collected at 2, 50, 100, 200, 300 and 400 K. This sample is cubic at room temperature, space group $Fm\bar{3}m$, in agreement with previous reports, including the oxygen deficient specimen [20-22]. The refinement of this sample in the paramagnetic region (300 and 400 K) only shows a slight oxygen deficiency yielding a chemical formula of $Sr_2CrMoO_{5.96}$. This result reveals the strong influence of the synthesis conditions on the final oxygen content of this sample and justifies to revisiting Sr_2CrMoO_6 properties.

The refinement at high temperature gives a value of 35% for the ASD which is closer to a single perovskite (50%) than to a fully ordered compound (0%). This high number of ASD may arise from the similar ionic radii of Cr^{3+} and Mo^{5+}, 0.615 and 0.61 Å, respectively [26]. In fact, attempts to refine the oxygen *x*-coordinate always gave the value ¼ within the standard deviation. We have fixed this value in the last step of the refinement obtaining a similar quality of the fit. This result implies equal bond lengths for both B-sublattices.

Figure 2 shows the refinement of Sr_2CrMoO_6 at 2 K. At low temperature, the pattern reveals additional intensity on some superstructure peaks and a slight broadening of the peaks at high angles. Both features are linked to the appearance of a tetragonal distortion as previously reported for the oxygen deficient sample [22]. The origin of this tetragonal cell can be understood as resulting from cooperative tilts of the $B(B')O_6$ octahedra. Following the Glazer's terminology [27], the tilt system present in Sr_2CrMoO_6 at 2 K is the $a^0a^0c^+$. The combination of this tilting system and the rock-salt ordering at the B-site leads to a tetragonal cell with the *I4/m* space group [22,28].

The tetragonal distortion is very small and the $c/\sqrt{2}a$ ratio is only 0.9995 at 2 K indicating that the unit cell is still nearly cubic. The pattern at 50 K also shows the superstructure peaks arising from the oxygen shifts away from the cubic positions while there are no superstructure peaks of this type in the pattern taken at 100 K where the cell is metrically cubic.

The pattern in Fig. 2 exhibits as well additional intensity on some low angle Bragg peaks arising from the establishment of long-range magnetic ordering. The most intense magnetic contributions are observed at the (0 1 1) and (1 2 1) diffraction peaks (tetragonal cell). The absence of any additional Bragg peaks within the magnetic phase point to a magnetic propagation vector **k**=0. Due to the pseudocubic crystal structure, it is impossible to ascertain the spin direction from only powder diffraction. Thus in the refinement we assumed that the moments lie within the *xy*-plane. In order to model the magnetic structure we must take into account that this compound has two crystallographic sites occupied by two types of magnetic cations, Cr^{3+} and Mo^{5+}. Since the magnetic moment of Cr^{3+} (d^3-ion) should be about three times larger than the one of Mo^{5+} (d^1-ion) one can suppose that the main magnetic

contribution stems from the Cr^{3+} interactions. We were successful in modelling the magnetic structure as a G-type with antiferromagnetic interactions along the three directions. The magnetic form factor of Cr^{3+} was assumed for both sites and the magnetic moment was constrained to have the same value for both B and B'-sites. Hence, the refined moment can be considered as an average of the localized moments in these sites. A best discrepancy factor of R_{mag}~8% was reached for the diagram of Fig. 2 using this model. Our attempts to refine different magnetic moment values for B and B'-sites (as in the archetypical Sr_2FeMoO_6) or to use the two magnetic form factors of Cr^{3+} and Mo^{5+} preserving the nuclear stoichiometry always lead to unstable refinements.

The magnetic peaks are much broader than the nuclear peaks suggesting a short coherence length (*L*) for the magnetic phase. In order to evaluate *L*, we have refined a parameter in the magnetic phase accounting for the isotropic particle size broadening. The inset in Fig. 2 compares the accuracy of the fit with and without use of this parameter. The improvement is significant although the effect on the refined magnetic moment is minor. This parameter affects the Gaussian part of the pseudo-Voigt function used to model the peak shape [25] and yields an average grain size after applying the Scherrer equation. We obtained a value of only 57 Å for Sr_2CrMoO_6 indicating a small coherence length for the magnetic ordering. The magnetic contribution to the Bragg peaks is still noticeable in the pattern taken at 100 K where the sample is already cubic. This indicates that the magnetic ordering is not coupled to the structural transition as was found in other related DP [29].

3.1.2. $Sr_{2-x}La_xCrMoO_6$ samples.

The samples belonging to this series correspond to compounds having a

nominal e-doping. Refinements of the neutron data taken at high temperature do not reveal a significant oxygen deficiency for any of these samples, indicating that the addition of La improves the oxygen stoichiometry. $Sr_{1.9}La_{0.1}CrMoO_6$ is cubic at 300 K as Sr_2CrMoO_6 and shows a similar amount of ASD. At 2 K $Sr_{1.9}La_{0.1}CrMoO_6$ exhibits as well a tetragonal structure. The structural transition to the cubic phase occurs at higher temperatures than for the undoped compound. The pattern at 100 K still shows intensity on the superstructure peaks resulting from the cooperative tilting of the B(B')O_6 octahedra.

$Sr_{1.7}La_{0.3}CrMoO_6$ and $Sr_{1.5}La_{0.5}CrMoO_6$ are monoclinic over the whole temperature range (2 K – 300 K). They were refined in the $P2_1/n$ space group which is usually found in DP showing the tilt system $a^+b^-b^-$ [28]. However, the refinement reveals an increase of the ASD and the atomic occupations of both perovskite B-sites are practically equivalent within the experimental error. It is well known that single perovskites having the $a^+b^-b^-$ tilt system crystallize in an orthorhombic unit cell with *Pbnm* space group [27] as observed for instance in $LaCrO_3$. Our attempts to refine the neutron patterns of $Sr_{1.7}La_{0.3}CrMoO_6$ and $Sr_{1.5}La_{0.5}CrMoO_6$ using the orthorhombic cell of a single perovskite did not succeed. This result may suggest a short range ordering of Cr and Mo atoms not observed by diffraction techniques but strong enough to favour the formation of the monoclinic cell.

Detailed results of the refinements are given in Tables 1 to 4. It can be seen that the unit cell volume of the $Sr_{2-x}La_xCrMoO_6$ series expands with increasing doping ratio. This is true in spite of La^{3+} being smaller than Sr^{2+} [26]. Accordingly, the average B(B')-O bond lengths rise with increasing doping in agreement with an effective electron injection into the transition metal *d* bands as observed in related compounds [18,30]. Unfortunately, the large disorder does not allow determining the

specific atom, Cr or Mo, which receives the additional electronic density and both B-O distances exhibit similar values.

Figure 3(a) shows the neutron patterns of the three samples at low temperature. All samples show the same magnetic peaks observed in the parent compound. The intensity of the magnetic peaks seems to increase as the doping ratio does. However, the refined magnetic moment remains almost constant along the series (see Table 2) and our results reveal that what really happens is an increase of *L*. It may be related to an increase of the ASD which leads to an enhancement of Cr-O-Cr interactions favouring the increase of the coherence length for the magnetic phase and giving rise to sharper magnetic peaks.

3.1.3. $Sr_{2-x}La_xCr_{1+x/2}Mo_{1-x/2}O_6$ samples.

These samples show the orthorhombic cell, space group *Pbnm*, typical of a single perovskite with the mentioned $a^+b^-b^-$ tilt system [27]. In fact, this is the structure found in $LaCrO_3$, one of the end points of this series, so this result cannot be considered as unexpected. The patterns could be refined as well using a monoclinic cell as for the $Sr_{2-x}La_xCrReO_6$ ($x \geq 0.3$) samples but in this case there is no improvement in the refinement and the value of β angle remains at 90º indicating an orthogonal lattice. This suggests that the Cr-excess present in these $Sr_{2-x}La_xCr_{1+x/2}Mo_{1-x/2}O_6$ samples favours the random distribution of Cr and Mo atoms at the B-sites. The orthorhombic distortion increases as the La (and Cr) content increases as can be inferred from the data of Tables 1-4. Another interesting feature is the evolution of the unit cell volume along this series. It decreases with increasing the La content due to the different ionic size for La^{3+} and Sr^{2+}. This difference is not compensated by an effective e-doping due to the Cr-excess. Therefore, the unit cell

shrinks although B-O distances slightly increase as Cr^{3+} is slightly bigger than Mo^{5+} [26]. The comparison between both series in the whole temperature range is summarized in Fig. 4 where the different space groups realized in these systems are also indicated. This result together with previous reports on doping in FeRe- and FeMo-based DP [18,30] points out that an effective e-doping induces an expansion of the unit cell whereas the simple replacement of Sr^{2+} by La^{3+} would lead to a volume reduction as is observed in the present system and in $Sr_{2-x}La_xFe_{1+x/2}Re_{1-x/2}O_6$ compounds [31].

Figure 3(b) shows the neutron patterns of these samples at 2 K. They exhibit the same magnetic peaks already observed for the first series of samples. As in the $Sr_{2-x}La_xCrMoO_6$ compounds, the intensity of the magnetic peaks becomes more noticeable with higher La-content. The refinements reveal in this case, however, that both the ordered magnetic moment and the correlation length L increase with increasing La content. This can be ascribed to the Cr-excess in the chemical composition which stimulates Cr-O-Cr superexchange interactions leading to higher magnetic moments and an enlarged *L*.

3.2. Magnetic transition.

The thermal evolution of the magnetic ordering was studied from a set of neutron diffraction patterns collected between 2 and 320 K with λ=2.52 Å. The magnetic structure is stable from 2 K up to T_N for all compounds. The temperature evolution of the first magnetic peak is illustrated for all samples in Fig. 5. The peak is indexed as (1 0 1) and (1 0 1)+(0 1 1) for the tetragonal and monoclinic cells respectively. The magnetic contribution becomes visible around 135 K for our undoped sample. In both series the temperature for the emerging of the magnetism is

directly related to the La content in the sample. For instance, the magnetic contribution appears at similar temperatures for $Sr_{1.7}La_{0.3}CrMoO_6$ and $Sr_{1.7}La_{0.3}Cr_{1.15}Mo_{0.85}O_6$ (or for $Sr_{1.5}La_{0.5}CrMoO_6$ and $Sr_{1.5}La_{0.5}Cr_{1.25}Mo_{0.75}O_6$). This result may be understood as a consequence of the strong structural disorder in both series favouring the Cr-O-Cr superexchange interactions which seem the main factor to develop long-range magnetic ordering for the present systems. The Cr-excess in the $Sr_{1.5}La_{0.5}Cr_{1.25}Mo_{0.75}O_6$ compounds enhances the intensity of the magnetic peaks in agreement with the structural refinement presented in the previous section.

3.3. Macroscopic magnetic properties.

The magnetic properties were also studied by means of macroscopic measurements. Fig. 6 shows the temperature dependence of magnetization for Sr_2CrMoO_6 at 5 KOe in zero field cooled (ZFC) and field cooled (FC) conditions. The magnetization exhibits a cusp around 60 K and magnetic irreversibility between ZFC and FC conditions appears at lower temperatures. This result is different to the one obtained for the oxygen deficient sample where the magnetic irreversibility was found above room temperature [22]. Therefore, this finding suggests that magnetism in $Sr_2CrMoO_{6-\delta}$ appears at lower temperature as the samples become more stoichiometric in oxygen (or δ decreases). The differences in oxygen content may be the reason for the different properties reported in the literature [19-22].

The inset of the figure shows the isothermal magnetization at selected temperatures. Sr_2CrMoO_6 exhibits a hysteresis loop with a large coercive field at 5 K and it does not achieve magnetic saturation at 5 T. Moreover the value of the magnetic moment at this field is very low in agreement with previous reports and in disagreement with a ferrimagnetic model of two sublattices with different ratios of

Cr and Mo atoms. This is another indication that not all atoms in the compound participate in the long range magnetic ordering. Regarding the neutron results, magnetism arising from magnetic clusters with short coherence lengths seems to be more plausible to account for these properties. The loops at higher temperatures show a strong decrease of the coercivity and a diminution for the ferromagnetic contribution. A very slight contribution of the later is still noticeable in the measurement at 300 K. We assign this parasitic signal to non-stoichiometric regions in our sample as the oxygen deficient compound show significant ferromagnetism at room temperature [22].

Figure 7 shows the magnetic hysteresis loops collected at 5 K for $Sr_{1-x}La_xCrMoO_6$ and $Sr_{1-x}La_xCr_{1+x/2}Mo_{1-x/2}O_6$ series. All loops show similar properties with strong coercive fields and without magnetic saturation at 50 KOe. Moreover, all samples exhibit low values of the magnetic moment at 5 T. This moment decreases with increasing the La-content. This feature may be related to the increase of magnetic coherence in the antiferromagnetic phase induced by the increase of ASD. Accordingly, the difference between $Sr_{1.7}La_{0.3}CrMoO_6$ and $Sr_{1.5}La_{0.5}CrMoO_6$ is very small reflecting the similar random occupation of B and B'-sites for both samples. The differences present between x=0 and x=0.1, with similar ASD, might suggest a role of the e-doping as observed in related systems [7-15].

Figure 8 shows the temperature dependence of the ac magnetic susceptibility for both series up to 350 K. In Fig. 8(a), Sr_2CrMoO_6 exhibits a strong peak at ~60 K in agreement with the previous magnetization measurements and a previous report [21]. Above this temperature, the susceptibility decays as temperature does but the compound does not behave as a conventional paramagnet and a small shoulder is noticeable around 200 K. Accordingly, the inverse of the susceptibility (not shown

here) does not obey a Curie-Weiss law. The complicated behaviour of the magnetic susceptibility is more evident for the rest of the samples. $Sr_{1.9}La_{0.1}CrMoO_6$ shows two peaks in the susceptibility curve whereas several anomalies are noticeable for $Sr_{1.7}La_{0.3}CrMoO_6$ and $Sr_{1.5}La_{0.5}CrMoO_6$ samples. Two trends are observed in this series upon increasing the La-content. On the one hand, the susceptibility magnitude decreases and on the other, the high temperature anomaly is shifted to higher temperatures. Figure 8(b) shows the same measurements for $Sr_{1-x}La_xCr_{1+x/2}Mo_{1-x/2}O_6$ compounds. These samples also show several anomalies in the susceptibility curves with the first magnetic anomaly appearing at higher temperature as the La-content is increased. The temperature of this first anomaly agrees with the appearing of magnetic contribution in the neutron patterns and it can be related to the onset of the antiferromagnetic ordering (compare Fig. 8 to 5).

The presence of several magnetic anomalies has also been observed in related DP with a high degree of structural disorder [17,31]. It supports a scenario of magnetically inhomogeneous samples. This inhomogeneity would arise from the strong ratio of ASD giving rise to different competitive magnetic interactions: Cr^{3+}-O-Cr^{3+}, Mo^{5+}-O-Mo^{5+} and Cr^{3+}-O-Mo^{5+}. In the case of e-doped compounds, the partial reduction of one of these cations (probably the Mo^{5+} according to the related FeMo-based DP [32]) should further complicate the scenario. It is difficult to identify the strongest magnetic interaction although our results suggest that it could be the Cr^{3+}-O-Cr^{3+} interaction. This follows from the fact that our samples show the magnetic contribution below room temperature where T_N has been reported for $LaCrO_3$ which possesses only this type of interactions [24].

It is likely that these samples contain regions with a cationic ordering close to the ideal double perovskite whereas ASD could be accumulated in other parts of the

compound where the Cr-O-Cr superexchange interaction is predominant, more or less diluted by the presence of adjacent Mo atoms. These Cr-rich regions begin to order at higher temperatures and regions with lower amount of ASD become ordered at lower temperatures. The different regions, with similar nuclear structure, have nanometric sizes explaining the broadening of the magnetic peaks observed in the neutron diffraction patterns. It is possible that a part of the material does not even reach a magnetic ordered state remaining in a cluster-glass state. Such a scenario could support the presence of several anomalies in the susceptibility curves and the observed magnetic irreversibility between ZFC and FC curves.

4. CONCLUSIONS.

We were successful in preparing $Sr_{2-x}La_xCrMoO_6$ ($x \leq 0.5$) and $Sr_{2-x}La_xCr_{1+x/2}Mo_{1-x/2}O_6$ ($x \leq 1$) compounds. The first series of samples belong to the family of double perovskites although they show an almost complete disorder at the B-site for $x \geq 0.3$. The second set of compounds crystallizes under the structure of a single perovskite with Cr and Mo atoms randomly placed at the B-site. Only Sr_2CrMoO_6 and $Sr_{1.9}La_{0.1}CrMoO_6$ present a cubic structure at room temperature and a tetragonal distortion at low temperature. The rest of the samples are pseudocubic showing monoclinic (e-doped samples) or orthorhombic (non-doped compounds) distortions.

All samples undergo an antiferromagnetic ordering at low temperature. The magnetic structure is defined by the propagation vector **k**= 0 in all cases and it can be modeled by the antiferromagnetic ordering of Cr^{3+} magnetic moments with a G-type structure. The low ordered magnetic moment indicates that not all magnetic atoms participate in the long range ordering probably due to the dilution effects produced

by the solid solution with Mo atoms which is partial in the case of e-doped samples. Moreover, the magnetic peaks are broad revealing a short coherence length. This coherence increases with increasing the La-content in both series and it is higher for the $Sr_{2-x}La_xCr_{1+x/2}Mo_{1-x/2}O_6$ compounds what it is likely due to the excess of Cr in the chemical composition favoring the Cr-O-Cr interactions.

Consequently, competitive interactions and magnetically inhomogeneous samples are expected for both series due to the structural disorder. Magnetic measurements confirm this feature since the susceptibility curves reveal several magnetic anomalies that have been ascribed to the presence of nanometric clusters with small differences in the atomic Cr/Mo ratio giving rise to diversity in the strength of the magnetic interactions.

Finally, electron doping is possible for Sr_2CrMoO_6 as deduced for the existence of $Sr_{2-x}La_xCrMoO_6$ single phase showing expanded unit cells as observed in other e-doped systems [18,30]. The system exhibits an increase of the magnetic transition temperature with increasing La content. However, the comparison with the $Sr_{2-x}La_xCr_{1+x/2}Mo_{1-x/2}O_6$ series shows that it is very difficult to differentiate e-doping effects from the effects induced by the growing number of Cr^{3+}-O-Cr^{3+} superexchange interactions resulting from the increase of ASD with increasing x.

Acknowledgements.

The authors acknowledge financial support from CICyT (project FIS08-03951 and MAT2007-61621) and DGA (CAMRADS). We also thank ILL and SPINS for neutron beam time allocation.

References.

[1] Bibes M and Barthelemy A 2007 *IEEE transactions of Electron Devices* **54** 1003.

[2] Kobayashi K I, Kimura T, Sawada H, Terakura K and Tokura Y 1998 *Nature* **395** 677.

[3] Galasso F, Douglas F C and Kasper R 1966 *J. Chem. Phys.* **44** 1672.

[4] Blasco J, Sánchez M C, Pérez-Cacho J, García J, Subías G and Campo J 2002 *J. Phys. Chem. Sol.* **63** 781.

[5] Retuerto M, Martínez-Lope M J, García-Hernández M and Alonso J A 2009 *J. Phys.: Condens. Matter* **21** 186003.

[6] Manako T, Izumi M, Kobayashi K, Kawasaki M and Tokura Y 1999 *Appl. Phys. Lett.* **74** 2215.

[7] Navarro J, Frontera C, Balcells Ll, Martínez B and J. Fontcuberta J, *Phys. Rev. B* 2001 **64** 092411.

[8] Rubí D, Frontera C, Nogués J and Fontcuberta J 2004 *J. Phys.: Condens. Matter* **16** 3173.

[9] Hemery E K, Williams G V M and Trodahl H J 2006 *Phys. Rev. B* **74** 054423.

[10] Linden J, Shimada T, Motohashi, Yamauchi H and Karpinnen M 2004 Sol. State Comm. **129** 129.

[11] Serrate D, De Teresa J M, Blasco J, Ibarra M R, Morellón L and Ritter C 2002 *Appl. Phys. Lett.* **80** 4573.

[12] Navarro J, Nogués J, Muñoz J S and Fontcuberta J 2003 Phys. Rev. B **67** 174416.

[13] Sánchez D, Alonso J A, García-Hernández M, Martínez-Lope M J, Casais M T and Martínez J L 2003 *J. Mater. Chem.* **13** 1771.

[14] Philipp J B, Majewski P, Alff L, Erb A, Gross R, Graf T, Brandt M S, Simon J, Walther T, Mader W, Topwal D and Sarma D D 2003 *Phys. Rev. B* **68** 144431.

[15] Azad A K, Eriksson S G, Khan A, Svedlindh P and Irvine J T S 2008 *Phys. Rev. B* **77** 064418.

[16] Blasco J, Michalik J M, García J, Subías G and De Teresa J M 2007 *Phys. Rev. B* **76** 144402.

[17] Michalik J M, De Teresa J M, Blasco J, Ritter C, Algarabel P A, Ibarra M R and Kapusta Cz 2009 J. Phys.: Condens. Matter submitted.

[18] Blasco J, Rodríguez-Velamazán J A, Ritter C, Sesé J, Stankiewicz J and Herrero-Martín J 2009 *Sol. State Sci.* **11** 1535.

[19] Moritomo Y, Xu Sh, Machida A, Akimoto T, Nishibori E, Takata M, Sakata M 2000 Phys. Rev. B **61** R7827.

[20] Arulraj A, Ramesha K, Gopalakrishnan J, Rao CNR 2000 J. Sol. State Chem. 155 233

[21] Chan T S, Liu R S, Guo G Y, Hu S F, Lin J G, Lee J F, Jang L Y, Chang C R, Huang C Y 2004 Sol. State Comm. 131 531.

[22] Blasco J, Ritter C, Morellón L, Algarabel P A, De Teresa J M, Serrate D, García J and Ibarra M R 2002 *Sol. State Sci.* **4** 651.

[23] Li Q F, Zhu X F, Chen L F 2008 *J. Phys.:Condens. Matter* **20** 255230.

[24] Sakai N, Fjellvag H, Hauback B C 1996 *J. Sol. State Chem.* **121** 202.

[25] Rodríguez-Carvajal J 1992 *Physica B* **192**, 55; available at www.ill.eu/sites/fullprof/

[26] Shannon R D 1976 *Acta Cryst. A* **32** 751.

[27] Glazer A M 1975 *Acta Cryst. A* **31** 756.

[28] Woodward P M 1997 *Acta Cryst. B* **53** 32.

[29] Ritter C, Blasco J, De Teresa, J M, Serrate D, Morellón L, García J and Ibarra M R 2004 *Sol. State Sci.* **6** 419.

[30] Navarro J, Frontera C, Balcells Ll, Martínez B and Fontcuberta J 2001 Phys. Rev. B **64** 09241.

[31] Blasco J, Sesé J, Rodríguez-Velamazán J A, Ritter C and Herrero-Martín J 2009 *J. Phys.:Condens. Matter* **21** 216008.

[32] Navarro J, Fontcuberta J, Izquierdo M, Avila J and Asensio M C 2004 *Phys. Rev. B* **70** 054423.

Sample	**Sr_2CrMoO_6**	**$Sr_{1.9}La_{0.1}CrMoO_6$**	**$Sr_{1.7}La_{0.3}CrMoO_6$**	**$Sr_{1.5}La_{0.5}CrMoO_6$**	**$Sr_{1.7}La_{0.3}Cr_{1.15}Mo_{0.85}O_6$**	**$Sr_{0.5}La_{1.5}Cr_{1.25}Mo_{0.75}O_6$**	**$SrLaCr_{1.5}Mo_{0.5}O_6$**
Space group	*$Fm\bar{3}m$*	*$Fm\bar{3}m$*	*$P2_1/n$*	*$P2_1/n$*	*Pbnm*	*Pbnm*	*Pbnm*
a (Å)	7.8278(2)	7.8312(3)	5.5440(2)	5.5497(3)	5.5350(8)	5.5345(6)	5.5322(4)
b (Å)	-	-	5.5523(2)	5.5599(3)	5.5272(4)	5.5200(4)	5.5026(4)
c (Å)	-	-	7.8130(2)	7.8188(3)	7.8142(9)	7.8094(9)	7.7954(8)
β (Deg.)	-	-	90.33(1)	90.39(1)	-	-	-
Vol/Z ($Å^3$)	59.95(1)	60.03(1)	60.12(1)	60.31(1)	59.76(1)	59.64(1)	59.33(1)
R_{Bragg} (%)	3.1	1.9	2.9	2.9	2.1	2.2	3.4
R_{wp} (%)	7.0	7.8	5.8	5.7	6.1	6.1	7.2

Table 1. Lattice parameters, unit cell volume per unit formula (Z=8 for the cubic cell and Z=4 for the rest of the cells) and reliability factors (defined as in ref. 25) obtained from the neutron refinements at 300 K. Numbers in parentheses refer to standard deviations of the last significant digits.

Sample: AA' BB'O$_6$	**Sr_2 $CrMoO_6$**	**$Sr_{1.9}La_{0.1}$ $CrMoO_6$**	**$Sr_{1.7}La_{0.3}$ $CrMoO_6$**	**$Sr_{1.5}La_{0.5}$ $CrMoO_6$**	**$Sr_{1.7}La_{0.3}$ $Cr_{1.15}Mo_{0.85}O_6$**	**$Sr_{0.5}La_{1.5}$ $Cr_{1.25}Mo_{0.75}O_6$**	**SrLa $Cr_{1.5}Mo_{0.5}O_6$**
Space group	*I4/m*	*I4/m*	*$P2_1/n$*	*$P2_1/n$*	*Pbnm*	*Pbnm*	*Pbnm*
a (Å)	5.5272(2)	5.5292(4)	5.5301(2)	5.5369(3)	5.5301(4)	5.5320(2)	5.5274(2)
b (Å)	-	-	5.5393(2)	5.5472(3)	5.5159(2)	5.5093(2)	5.4958(2)
c (Å)	7.8131(6)	7.8163(9)	7.7940(2)	7.8000(3)	7.8013(6)	7.7886(4)	7.7716(4)
β (Deg.)	-	-	90.36(1)	90.40(1)	-	-	-
Vol/Z (Å^3)	59.67(1)	59.74(1)	59.83(1)	60.04(1)	59.49(1)	59.38(1)	59.02(1)
$\mu_{B,B'\text{-site}}$ (μ_B)	1.03(3)	1.02(3)	1.04(2)	1.15(3)	1.14(2)	1.39(2)	1.86(2)
L **(**Å)	57(4)	69(6)	175(15)	240(23)	211(18)	283(21)	387(32)
R_{Bragg} (%)	2.4	1.8	2.4	2.8	2.1	2.1	3.2
R_{mag}(%)	8.2	8.6	8.5	6.2	11.1	5.8	2.6
R_{wp} (%)	6.7	6.6	5.7	5.9	5.3	5.9	6.1

Table 2. Lattice parameters, unit cell volume per unit formula (Z=4 in all cases), refined magnetic moment, coherence length of the magnetic phase and reliability factors (defined as in ref. 25) obtained from the neutron refinements at 2 K. Numbers in parentheses refer to standard deviations of the last significant digits.

Sample: AA'BB'O$_6$		**Sr_2CrMoO_6**	**$Sr_{1.9}La_{0.1}CrMoO_6$**	**$Sr_{1.7}La_{0.3}CrMoO_6$**	**$Sr_{1.5}La_{0.5}CrMoO_6$**	**$Sr_{1.7}La_{0.3}Cr_{1.15}Mo_{0.85}O_6$**	**$Sr_{0.5}La_{1.5}Cr_{1.25}Mo_{0.75}O_6$**	**$SrLaCr_{1.5}Mo_{0.5}O_6$**
Sr/La:	x	¼	¼	0.0018(25)	0.0008(18)	1.0010(21)	1.0014(14)	1.0026(2)
	y	¼	¼	0.0014(11)	0.0015(38)	0.0022(34)	0.0059(12)	0.0078(12)
	z	¼	¼	0.7530(13)	0.7561(10)	¼	¼	¼
B(Å^2)		0.84(4)	0.91(4)	0.84(3)	0.94(3)	0.95(3)	0.92(3)	0.94(4)
O1:	x	0.25*	0.25*	0.2508(29)	0.2595(25)	0.0241(15)	0.0359(11)	0.0509(9)
	y	0	0	0.2512(27)	0.2616(36)	0.4949(43)	0.4991(15)	0.4999(17)
	z	0	0	0.9918(17)	0.9796(9)	¼	¼	¼
O2:	x	-	-	0.2433(28)	0.2460(27)	0.7452(27)	0.7466(24)	0.7454(18)
	y	-	-	0.2427(26)	0.2431(37)	0.2527(26)	0.2532(26)	0.2571(13)
	z	-	-	0.5126(16)	0.5111(9)	0.0086(8)	0.0125(6)	0.0204(4)
O3:	x	-	-	0.9789(14)	0.9704(13)	-	-	-
	y	-	-	0.4924(15)	0.4997(44)	-	-	-
	z	-	-	0.7483(14)	0.7474(11)	-	-	-
B(Å^2)		0.61(3)	0.67(3)	0.56(2)	0.72(3)	0.70(2)	0.69(2)	0.72(4)
B_{site}: Cr/Mo		65/35	66/34	50/50	50/50	57.5/42.5	61.25/38.75	75/25
B'_{site}: Mo/Cr		65/35	66/34	50/50	50/50	-	-	-
B(Å^2)		0.28(6)	0.25(4)	0.14(4)	0.15(3)	0.18(3)	0.16(4)	0.15(3)
<B-O> (Å)		1.957	1.958	1.957(6)	1.968(7)	1.957(5)	1.959(5)	1.961(3)
<B'-O> (Å)		1.957	1.958	1.966(6)	1.966(7)	-	-	-
<B-O-B'> (º)		180	180	174.2(6)	171.4(7)	174.5(3)	172.2(3)	168.1(2)

Table 3. Refined fractional atomic coordinates, occupancies at B(B') sites (%Cr:%Mo) and temperature factors at 300 K. Average bond lengths and bond angles for B and B' sites. An average temperature factor was refined for all oxygen atoms and for atoms in B-sites. The atoms are placed in the following Wyckoff positions. La/Sr at (8c), Cr/Mo at (4a) and (4c), O at (24e) for the cubic cell. La/Sr at (4e), Cr/Mo at (2c) and (2d), O at (4e) for the monoclinic cell. La/Sr at (4c), Cr/Mo at (4b), O1 at (4c), O2 at (8d) for the orthorhombic cell. Asterisks denote fixed parameters in the last refinement (see text).

Sample: AA'		**Sr_2**	**$Sr_{1.9}La_{0.1}$**	**$Sr_{1.7}La_{0.3}$**	**$Sr_{1.5}La_{0.5}$**	**$Sr_{1.7}La_{0.3}$**	**$Sr_{0.5}La_{1.5}$**	**SrLa**
BB'O_6		**$CrMoO_6$**	**$CrMoO_6$**	**$CrMoO_6$**	**$CrMoO_6$**	**$Cr_{1.15}Mo_{0.85}O_6$**	**$Cr_{1.25}Mo_{0.75}O_6$**	**$Cr_{1.5}Mo_{0.5}O_6$**
Sr/La:	x	½	½	0.9999(14)	0.9993(14)	1.0002(10)	1.0012(7)	0.9993(6)
	y	0	0	0.0010(19)	0.0019(37)	0.0038(41)	0.0057(10)	0.0078(8)
	z	¼	¼	0.7571(9)	0.7591(9)	¼	¼	¼
B($Å^2$)		0.41(2)	0.57(2)	0.51(3)	0.54(4)	0.59(3)	0.59(3)	0.64(3)
O1:	x	0.2419(57)	0.2371(11)	0.2611(23)	0.2625(19)	0.0330(8)	0.0396(6)	0.0330(8)
	y	0.2581(61)	0.2639(11)	0.2603(52)	0.2633(51)	0.4961(12)	0.5001(12)	0.4970(11)
	z	0	0	0.5109(18)	0.9783(8)	¼	¼	¼
O2:	x	0	0	0.2438(24)	0.2428(20)	0.7472(14)	0.7468(15)	0.7416(7)
	y	0	0	0.2413(50)	0.2378(47)	0.2509(29)	0.2526(18)	0.2594(7)
	z	0.25*	0.25*	0.5109(18)	0.5122(9)	0.0121(4)	0.0158(3)	0.0241(3)
O3:	x	-	-	0.9742(14)	0.9682(13)	-	-	-
	y	-	-	0.4959(26)	0.4982(45)	-	-	-
	z	-	-	0.7483(9)	0.7471(10)	-	-	-
B($Å^2$)		0.26(2)	0.32(2)	0.37(2)	0.46(3)	0.05(2)	0.04(3)	0.05(4)
B_{sites}: Cr-Mo								
B($Å^2$)		0.07(3)	0.06(2)	0.04(3)	0.02(4)	0.05(2)	0.04(3)	0.05(4)
<B-O> (Å)		1.954(12)	1.959(2)	1.958(7)	1.965(7)	1.956(4)	1.957(3)	1.959(1)
<B'-O> (Å)		1.954(12)	1.954(2)	1.961(7)	1.965(7)	-	-	-
<B-O-B'> (º)		177.5(6)	175.9(1)	172.4(4)	170.4(7)	172.5(3)	170.6(3)	167.1(1)

Table 4. Refined fractional atomic coordinates, occupancies at B(B') sites (%Cr:%Mo) and temperature factors at 2 K. Average bond lengths and bond angles for B and B' sites. An average temperature factor was refined for all oxygen atoms and for atoms in B-sites. The atoms are placed as indicated in table 3. For the tetragonal cell: La/Sr at (4d), Cr/Mo at (2b) and (2a), O1 at (4e) and O2 at (8h). Asterisks denote fixed parameters in the last refinement (see text).

Figure Captions.

Figure 1. Detail of the x-ray patterns for $Sr_{2-x}La_xCrMoO_6$ samples (from top to bottom, x=0, 0.1, 0.2, 0.3, 0.5 and 0.7). The patterns are shifted for the sake of clarity and the asterisk indicates the peaks arising from secondary phases in the x=0.7 sample.

Figure 2. Rietveld refinement of the neutron pattern for $Sr_2CrMoO_{5.96}$ at 2 K. The observed (points) and calculated (line) intensity are plotted. The difference between them is at the bottom and the vertical lines indicate the allowed Bragg peak position. Inset: Detail of the Rietveld refinement with (bottom) and without (top) refinement of the isotropic size parameter.

Figure 3. The observed (points) and calculated (line) intensity of the neutron patterns for $Sr_{2-x}La_xCrMoO_6$ (a) and $Sr_{2-x}La_xCr_{1+x/2}Mo_{1-x/2}O_6$ (b) samples. The value of x is indicated for each measurement and the patterns are shifted upwards for the sake of clarity. The arrow marks the first magnetic peak.

Figure 4. Volume per formula unit vs temperature for the samples indicated in the figure. Points are experimental measurements. Continuous lines are guides for the eyes and broken lines separate experimental points with different crystal structures.

Figure 5. (a) Temperature evolution of the magnetic peak intensity for $Sr_{2-x}La_xCrMoO_6$ (left) and $Sr_{2-x}La_xCr_{1+x/2}Mo_{1-x/2}O_6$ (right) samples. The first magnetic peak was chosen for all samples corresponding to the (101) for a tetragonal cell –(101)+(011) for monoclinic and orthorhombic cells-.

Figure 6. Magnetization vs temperature at 5 KOe under FC and ZFC conditions for $Sr_2CrMoO_{5.96}$. Inset: Magnetic hysteresis loops at selected temperatures indicated in the plot.

Figure 7. Magnetic hysteresis loops at 5 K for $Sr_{2-x}La_xCrMoO_6$ (left) and $Sr_{2-x}La_xCr_{1+x/2}Mo_{1-x/2}O_6$ (right) samples.

Figure 8. In-phase component of the ac magnetic susceptibility for $Sr_{2-x}La_xCrMoO_6$ (left) and $Sr_{2-x}La_xCr_{1+x/2}Mo_{1-x/2}O_6$ (right) samples. The data for $Sr_{1.5}La_{0.5}CrMoO_6$ has been multiplied by ten for the sake of comparison.

Figure 1

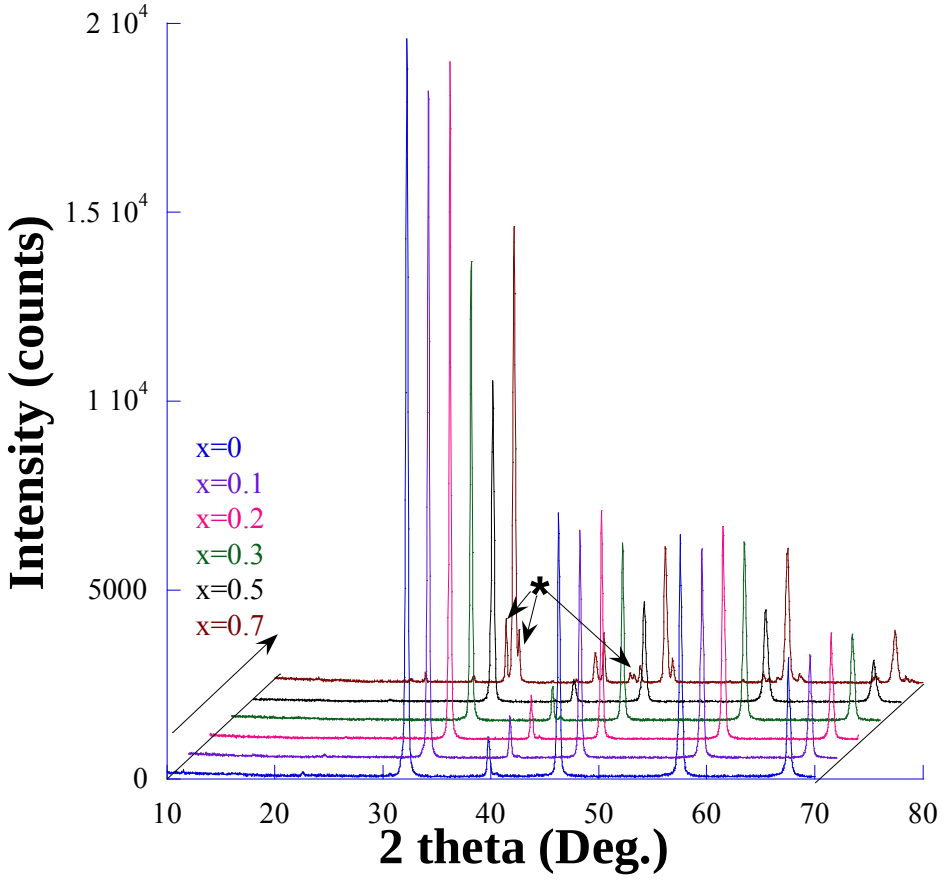
2 10^4
1.5 10^4
1 10^4
5000
0
Intensity (counts)
x=0
x=0.1
x=0.2
x=0.3
x=0.5
x=0.7
*
10
20
30
40
50
60
70
80
2 theta (Deg.)

Figure 2

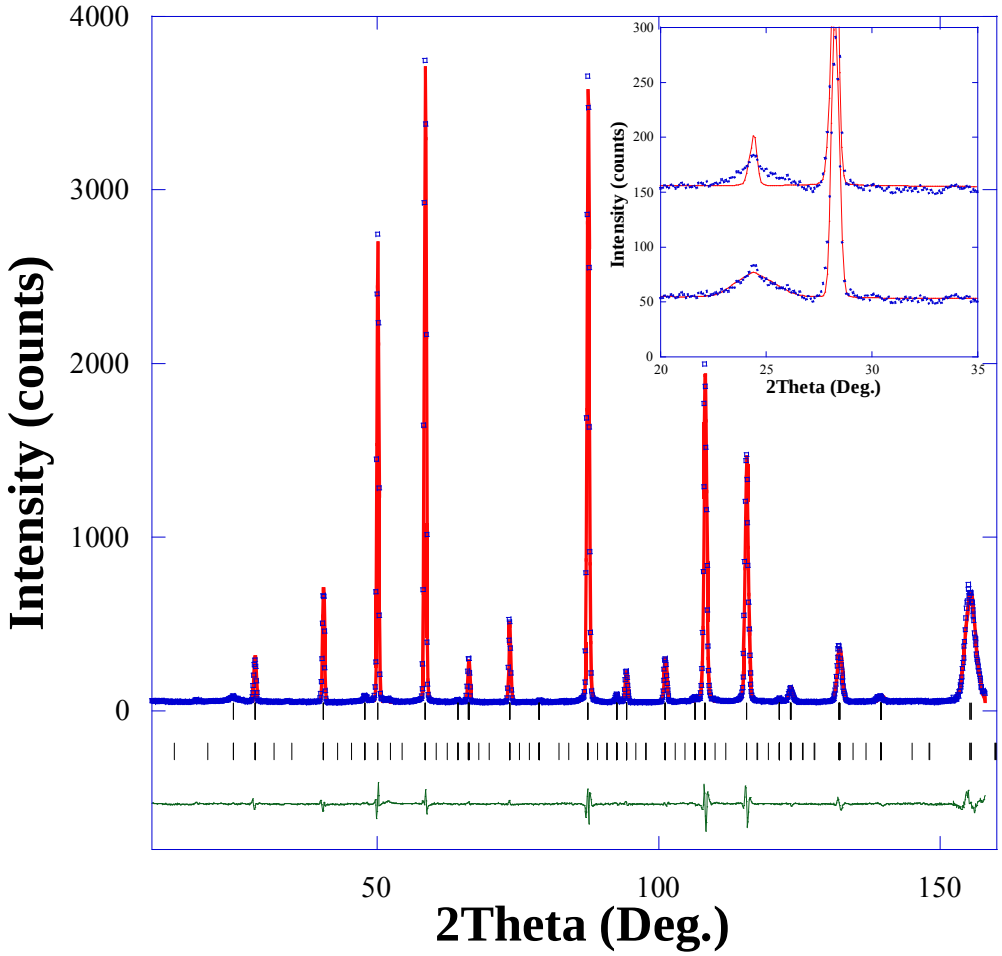
Intensity (counts)
4000
3000
2000
1000
0
50
100
150
2Theta (Deg.)
Intensity (counts)
300
250
200
150
100
50
0
20
25
30
35
2Theta (Deg.)

Figure 3

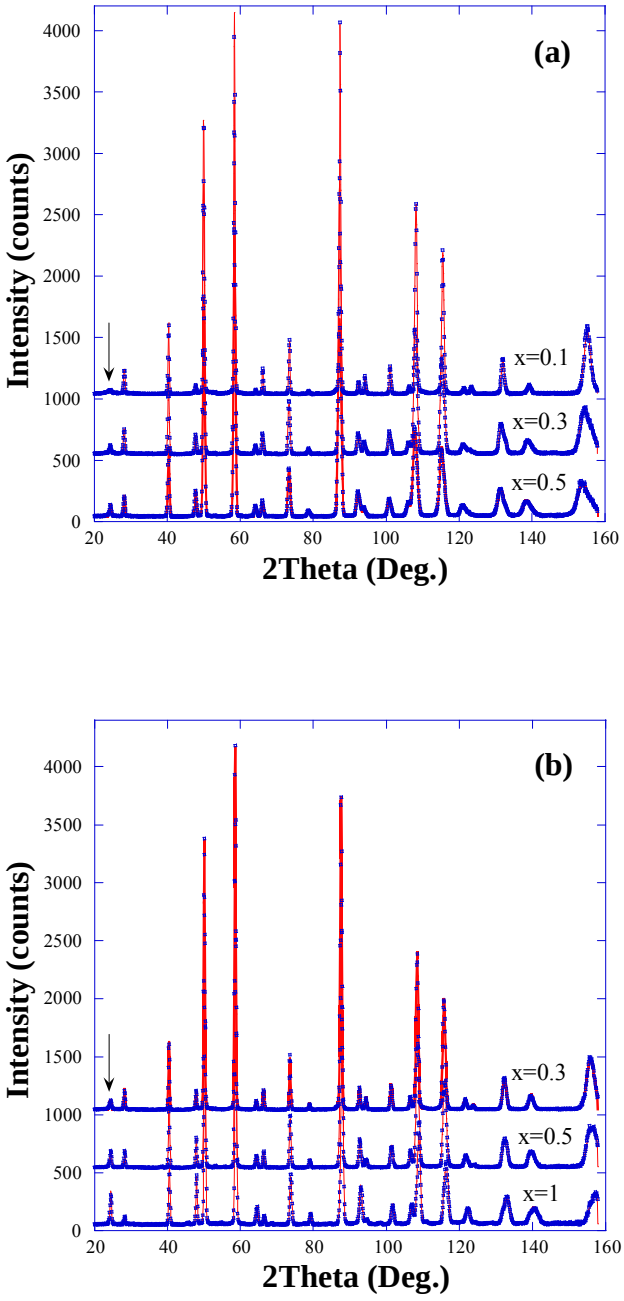
(a)
Intensity (counts)
2Theta (Deg.)
x=0.1
x=0.3
x=0.5
(b)
Intensity (counts)
2Theta (Deg.)
x=0.3
x=0.5
x=1

Figure 4

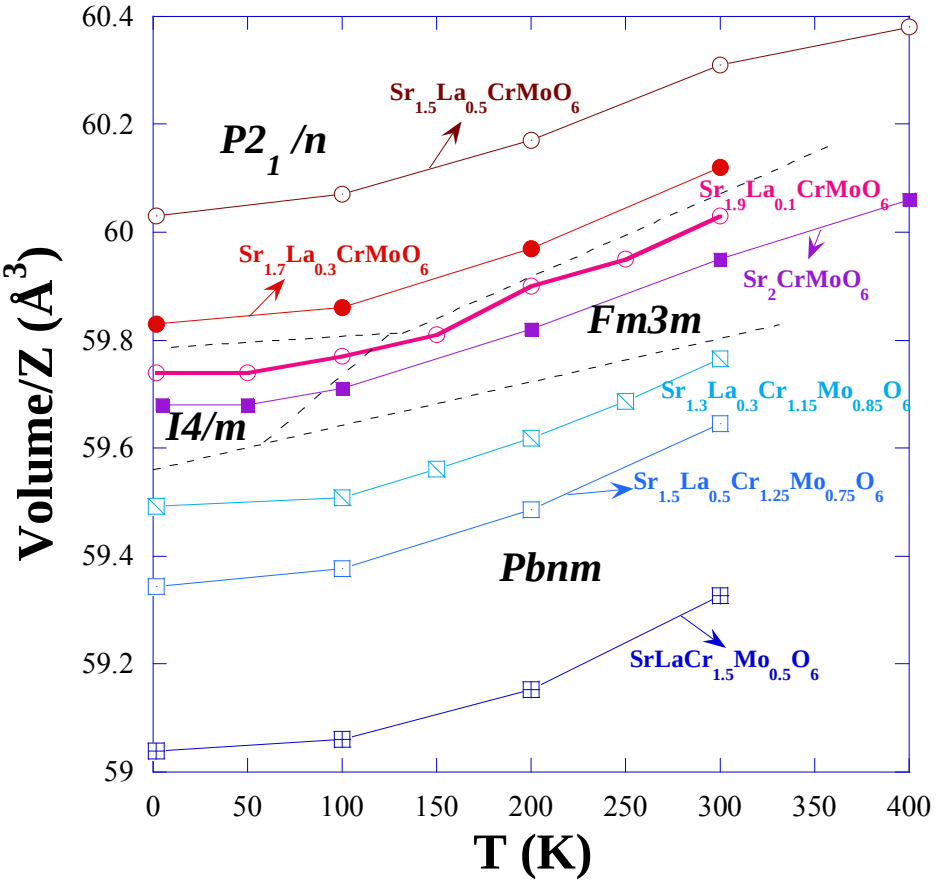
Volume/Z (Å^3)
T (K)
60.4
60.2
60
59.8
59.6
59.4
59.2
59
0
50
100
150
200
250
300
350
400
$Sr_{1.5}La_{0.5}CrMoO_6$
$P2_1/n$
$Sr_{1.9}La_{0.1}CrMoO_6$
$Sr_{1.7}La_{0.3}CrMoO_6$
Sr_2CrMoO_6
Fm3m
$Sr_{1.3}La_{0.3}Cr_{1.15}Mo_{0.85}O_6$
I4/m
$Sr_{1.5}La_{0.5}Cr_{1.25}Mo_{0.75}O_6$
Pbnm
$SrLaCr_{1.5}Mo_{0.5}O_6$

Figure 5

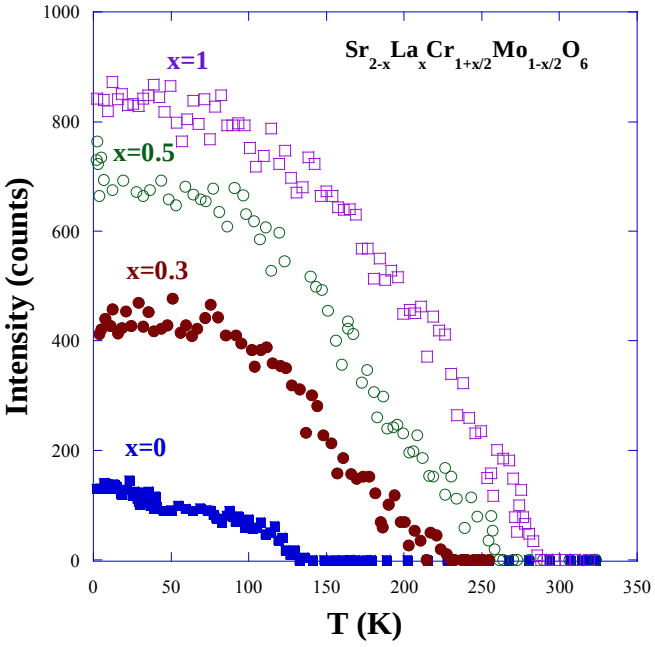
Sr2-xLaxCr1+x/2Mo1-x/2O6
x=1
x=0.5
x=0.3
x=0
Intensity (counts)
T (K)
0
200
400
600
800
1000
0
50
100
150
200
250
300
350

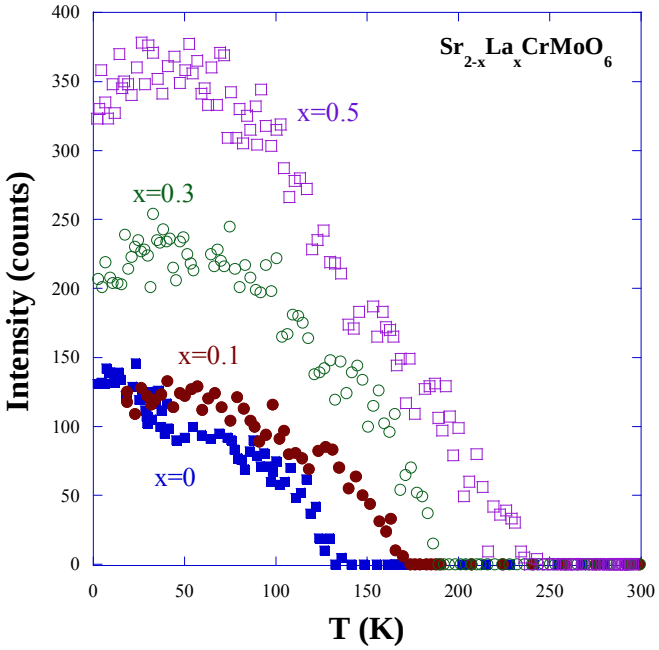
Sr2-xLaxCrMoO6
x=0.5
x=0.3
x=0.1
x=0
Intensity (counts)
T (K)
0
50
100
150
200
250
300
350
400
0
50
100
150
200
250
300

Figure 6

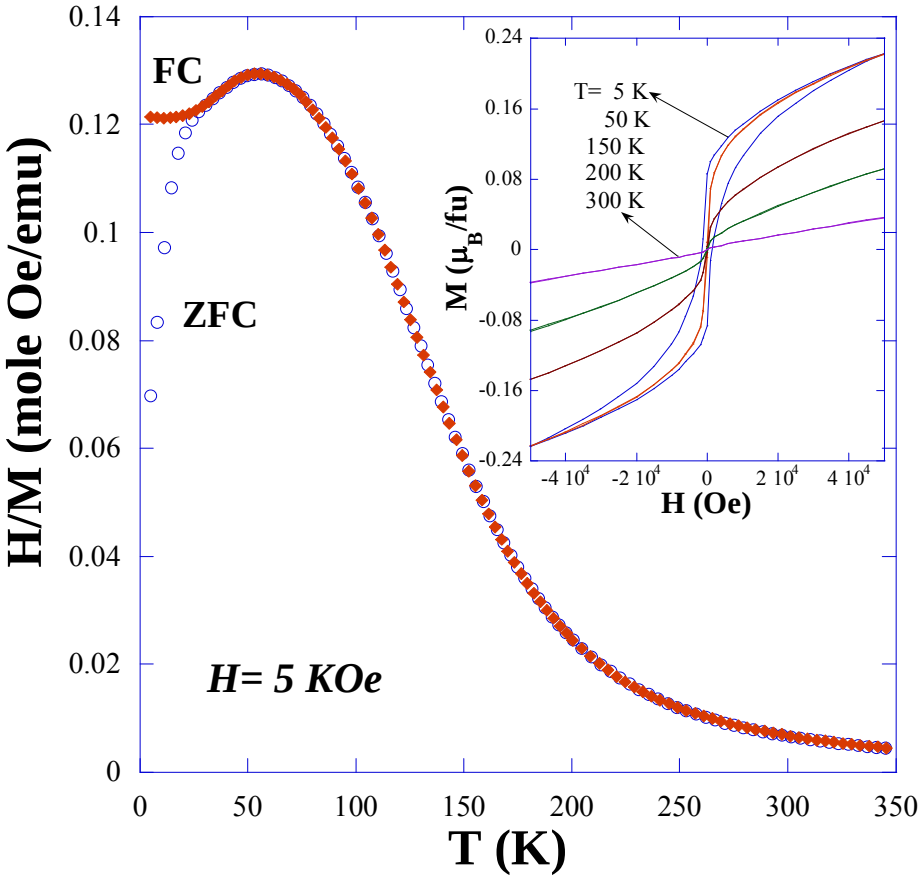
FC
ZFC
H= 5 KOe
H/M (mole Oe/emu)
T (K)
0.14
0.12
0.1
0.08
0.06
0.04
0.02
0
0
50
100
150
200
250
300
350
M (μB/fu)
H (Oe)
T= 5 K
50 K
150 K
200 K
300 K
0.24
0.16
0.08
0
-0.08
-0.16
-0.24
-4 10^4
-2 10^4
0
2 10^4
4 10^4

Figure 7

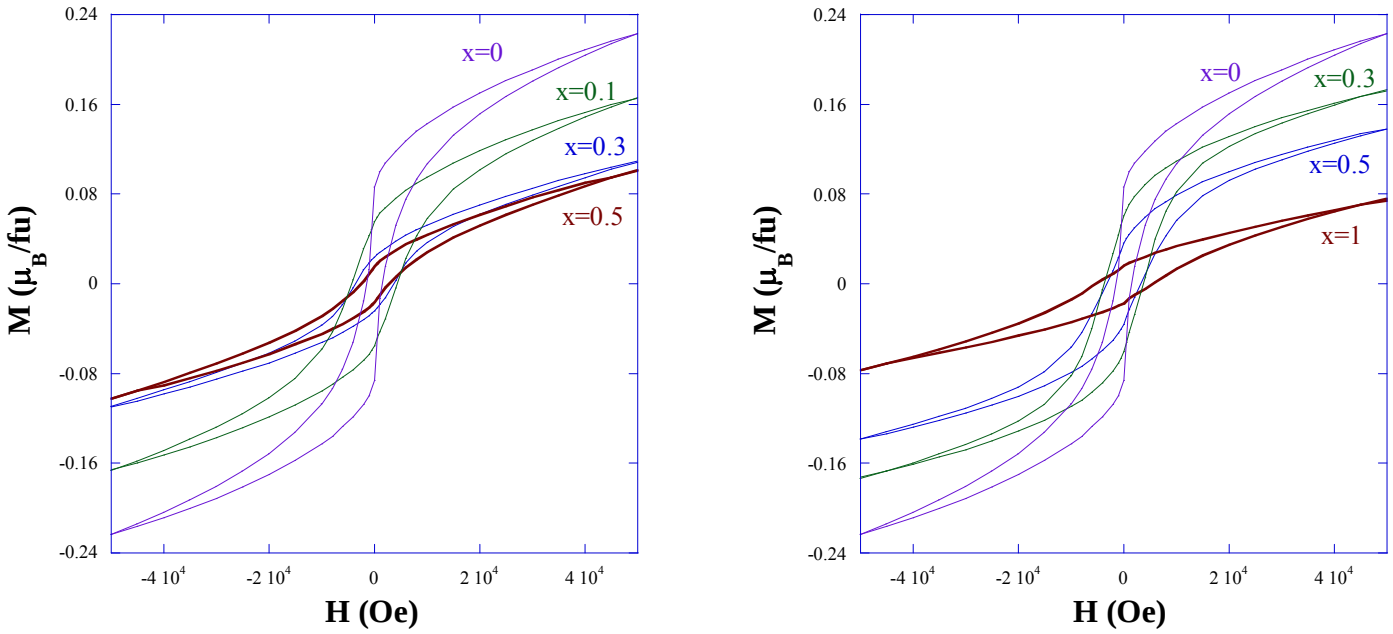
0.24
0.16
0.08
0
-0.08
-0.16
-0.24
M (μB/fu)
x=0
x=0.1
x=0.3
x=0.5
-4 10^4
-2 10^4
0
2 10^4
4 10^4
H (Oe)
0.24
0.16
0.08
0
-0.08
-0.16
-0.24
M (μB/fu)
x=0
x=0.3
x=0.5
x=1
-4 10^4
-2 10^4
0
2 10^4
4 10^4
H (Oe)

Figure 8

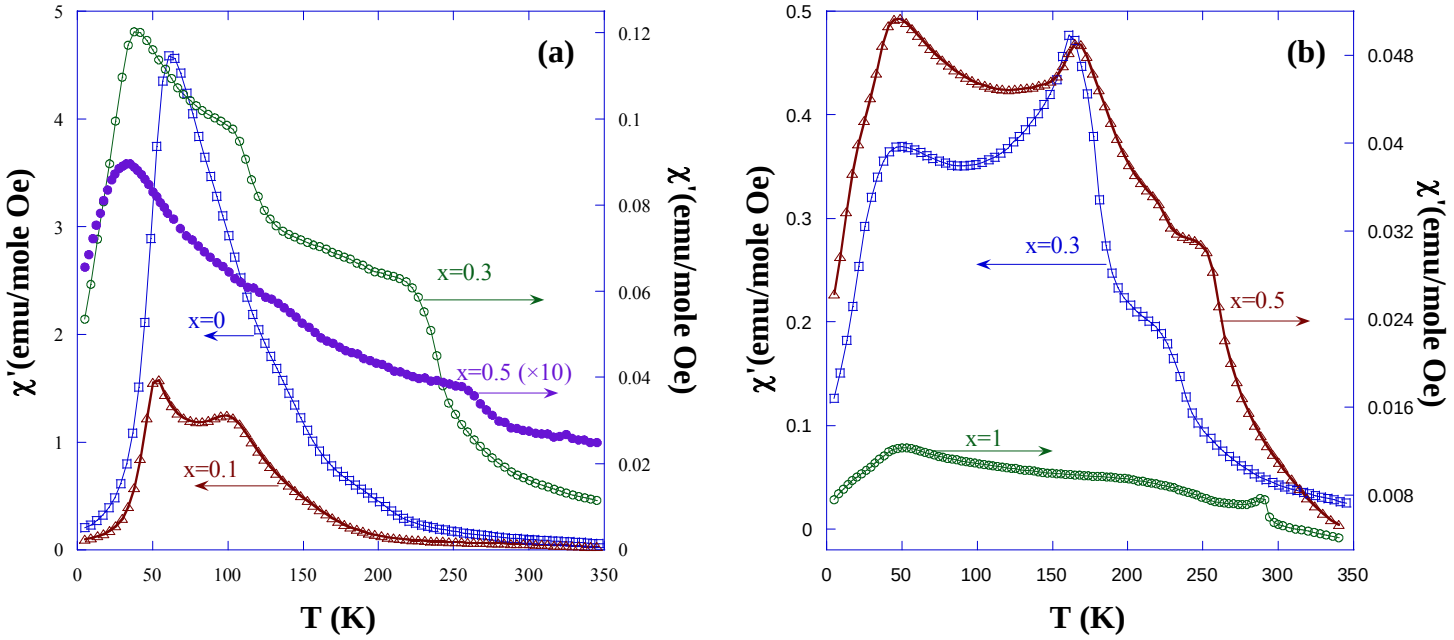
(a)
χ'(emu/mole Oe)
χ'(emu/mole Oe)
T (K)
x=0.3
x=0
x=0.5 (×10)
x=0.1
(b)
χ'(emu/mole Oe)
χ'(emu/mole Oe)
T (K)
x=0.3
x=0.5
x=1